Study of Hybrid MicroPattern Gas Detector with CsI Photocathode For Super Tau-Charm Factory RICH

Ping Li[a], Qian Liu[a,*], Jianbei Liu[b], Ming Shao[b], Zhiyong Zhang[b], Jianxin Feng[b], Anqi Wang[b], Baolin Hou[b,c], Lei Zhao[b], Hongbang Liu[d]

[a] *School of Physics, University of Chinese Academy of Sciences*
[b] *University of Science and Technology of China*
[c] *School of Information Engineering, Southwest University of Science and Technology*
[d] *GuangXi University*

Abstract

Super τ-Charm facility(STCF) is a future electron-position collider operating at τ-Charm energy region aimed to study hadron structure and spectroscopy. The baseline design of the STCF barrel particle identification(PID) detector in the momentum range up to 2 GeV/c is provided by a Ring Imaging Cherenkov Counter(RICH). The architecture of the RICH is an approximately focusing design with liquid perfluorohexane sealed in the quartz container as radiator and a hybrid combination of a CsI coated layers of THGEMs and a Micromegas as the photo-electron detector. A $16 \times 16\,\mathrm{cm}^2$ prototype with quartz radiator has been built and tested at DESY. It was stably operated with 10^5 effective gain. In this paper, the design, the performance, the reconstruction algorithm and the systematic error for single photon electron angular resolution in the aspect of RICH detectors are discusses.

Keywords: THGEM, MicroMegas, MPGD, STCF, RICH, PID

1. Introduction

The Super τ-Charm facility(STCF) is a future electron-positron collider, operating at center-of-mass energy region of 2 to 7 GeV and luminosity greater

*Corresponding author
Email address: liuqian@ucas.ac.cn (Qian Liu)

than $0.5 \times 10^{35}\,\mathrm{cm}^{-2}\mathrm{s}^{-1}$. The physical goals of STCF are to explore asymmetry of matter-antimatter (charged parity violation), the internal structure of hadrons and the nature of non-perturbative strong interactions, exotic particles and physics beyond Standard Model. Physics at the STCF will have demanding requirements on Particle Identification(PID), in particular on hadron PID at momenta up to $p = 2\,\mathrm{GeV/c}$.

Ring image Cherenkov(RICH) detector provides excellent PID capability in a wide range of momentum, and the concept has been used widely in high-energy experiments such as CLEOc[1], DELPHI[2] , ALICE[3], and COMPASS[4]. For STCF barrel PID, it is required that the detector is able to operated at high luminosity environment, the martial budge is less than 20%, and thickness of the detector is less than 20 cm. In order to meet those requirements, the hybrid micro-patter gas detector(MPGD) [5] based RICH detector with approximate focusing design is adopted as the baseline design.

The STCF RICH detector consists of a layer of CsI coated thick gas electron multipliers (THGEM)[6] and a resistive MicroMegas (MM)[7]

on a pad segmented anode. The MPGD detector has been demonstrated to be able to operate under a high counting rate with lower ion back-flow suppression while maintaining a high effective gain[5, 8]. The CsI coated THGEM acts as a reflective photo-cathode. The photoelectrons are pre-amplified by THGEM and transferred to MicroMegas. The total gain of the prototype RICH PID detector needs to reach $\approx 10^5$ to obtain a sufficient single-photon detection efficiency. The ions generated from multiplication are accelerated by the electric fields and eventually bombard the photo-cathode, which is called as Ion Back-Flow (IBF) and may cause severe aging problem. This hybrid design has been demonstrated to show an excellent IBF suppression [9], since the majority of the ions obtained from the multiplication are trapped by the MicroMegas stage and further suppressed by the THGEM layer.

For the momenta interested at the STCF, liquid perfluorohexane C_6F_{14} with quartz as container is chosen as the Cherenkov radiator. In order to evaluate the performance of the RICH PID detector, a prototype with quartz as radiator

is built. This work presents the performance of the hybrid MPGD prototype targeting the RICH PID detector. In section 2, the prototype and performance is described. The beam test setup is shown in section 3. In section 4, the performance of the system is presented, MC simulation is given in section 5. The conclusions are presented in section 6.

2. The hybrid MPGD based RICH prototype

To fulfill the PID requirements of the future STCF experiment, a similar RICH prototype has been designed and built except the radiator is pure quartz instead of liquid perfluorohexane.

The active area of the RICH prototype is about 16 cm × 16 cm. Fig.1 shows the prototype and the internal structure sketch:

- a 10 mm-thick quartz radiator of which both sides are polished and the transparency is about 60% at the wavelength of 180 nm. As demonstrated in the sketch, part of the Cherenkov radiation might be total internal reflected inside the quartz, thus the incident angle needs to be larger than 30° so the other part of the Cherenkov radiation can reach the CsI photo-cathode plane.

- A light propagation region of 88.2 mm is separated by the quartz radiator and the drift mesh. The drift mesh is made of 75 μm diameter gold plated tungsten wires and placed 4.8 mm away from the CsI coated THGEM and biased to a suitable voltage to maximize the extraction and collection efficiency of the converted photo-electron[10, 11].

- A CsI coated THGEM layer for UV photons conversion. THGEM is standard Printed Circuit Boards(PCB), manufactured with mechanical drilling pattern holes. The THGEM selected for this prototype is 0.4 mm thick, 0.4 mm diameter holes with 0.8 mm pitch and 50μm rim[12].

- A MicroMegas layer built on a pad segmented anode. The MicroMegas is produced using thermal bonding technology. It's made of stainless steel

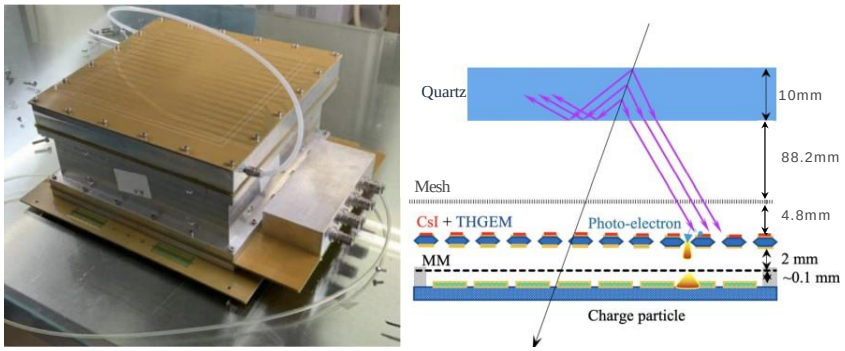

Figure 1: Overview of the RICH prototype. Left: the assembled RICH prototype. Right: sketch of the prototype.

mesh of 400 lines per inch (LPI) with 19 μm wires, stretched over the readout segmented anode. The gap of MicroMegas is 100 μm[13].

- A germanium coated PCB as the readout anode. The anode is segmented in 1024 square $5 \times 5\,\mathrm{mm}^2$ with 4.8 mm pitch, coated with a 400 nm germanium layer. The sheet resistivity is about 100 MΩ/sq[14].

The photo-electron generated by the CsI coated THGEM surface is guided into one of the holes and multiplied to a small factor of ≈ 10, and drifted across the 2 mm gap to the MicroMegas where the main multiplication occurs. In Fig.2 shows the typical gain achieved in Ar:CO_2=97:3 with single MicroMegas (in red), and THGEM combined MicroMegas (in blue). For the latter setup, the MM was fixed to 530 V which provides about 10^4 effective gain, and varied the THGEM voltage $\Delta V_{\mathrm{THGEM}}$ from 800 V to 1000 V. Up to 10^5 effective gain can be achieved and operated quietly for the hybrid combination, and the ion back flow of this setup is demonstrated to be less than 0.1%[7].

3. The Experiment Setup

The experiments were carried out at the DESY beam line, which uses a beam energy of up to 6.3 GeV electrons to cross the primary target. The primary targets are 7 μm thick carbon fibers, at which Bremsstrahlung photons

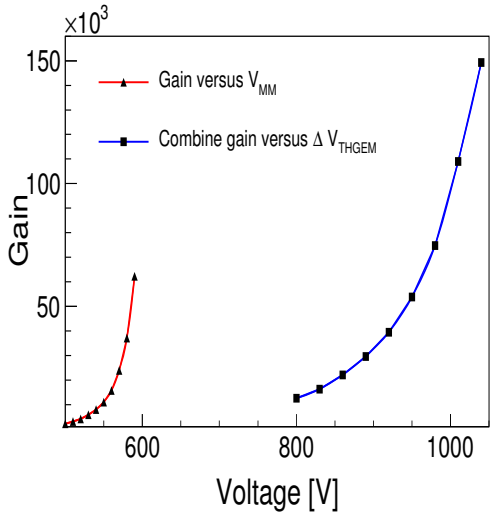

Figure 2: Effective Gain of MicroMegas and hybrid MicroMegas+THGEM versus high voltage. For hybrid setup, the MicroMegas was fixed to 530 V and varied the THGEM voltage.

are produced. These photons move towards a secondary target, also called conversion target, consisting of metal sheets of a few mm thickness and produce electron/positron pairs. Then the dipole magnet is placed behind to select the particle type and the momentum. During the test, the momentum of electron beam was set to 5 GeV/c and collimated within $1 \times 1\,\mathrm{cm}^2$ area.

Fig.3 shows the experimental setup. The trigger signal was generated by the two-fold time coincidence of plastic scintillator paddles with photo-multiplier tube readout, which was placed in the beam upstream with a sensitive area of $1 \times 2\,\mathrm{cm}^2$. The trigger rate was about 20 Hz during the running and spread to each system by the Trigger Logic Unit(TLU)[15].

The particle tracking system comprised three "back-to-back" MicroMegas detectors. The total sensitive area of each detector was $15 \times 15\,\mathrm{cm}^2$. Only the center area of $5 \times 5\,\mathrm{cm}^2$ was read out with a 400 μm pitch X/Y strips. The trackers were operated with a non flammable gas mixture of Ar/CO_2=97:3 and the average gain was close to 10^4. After installation, the onsite laser system was used to measure the global alignment of the tracking detectors. Then the

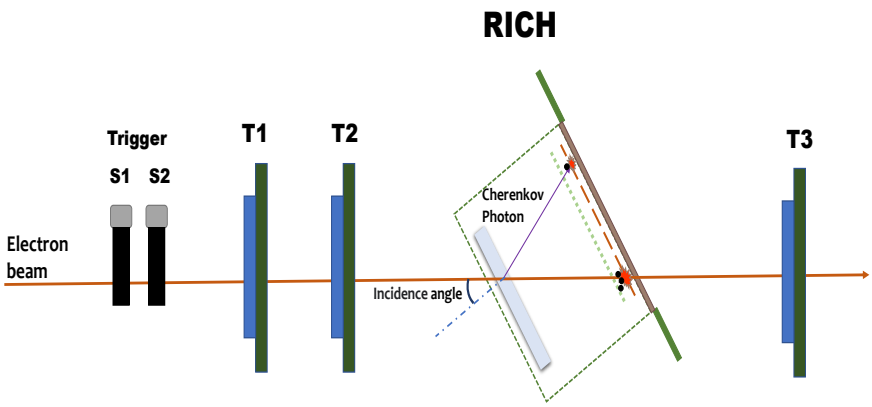

Figure 3: Schematic view of the beam line. From left to right: the two scintillators used for the trigger, the three MicroMegas composed the tracker system, and the RICH prototype rotated with an incident angle θ.

inter-module alignment was extracted using fitted tracks.

The RICH prototype chamber was placed along the beam line in between three tracker elements. The prototype was rotatable toward the direction of the electron beam to scan the different incident angle. During the experiments, a scan from 30° to 45° with 5° step were performed. For each scan, the prototype was translated to ensure the ionization signal and Cherenkov photo-electron signal were both recorded. The prototype was flushed with Ar/CO_2=97:3. The oxygen and water contamination rates of the flowing gas were monitored by an oxygen analyzer and a dew-point hygrometer.

The RICH signals, as well as those recorded from the tracker system were read out by the AGET based Front-End Electronics(FEE)[16] and Data Collection Modules(DCMs)[17]. The data acquisition was triggered by the scintillators coincidence signal. For each triggered event, the waveform (sampled in 512 bins of 25 μs each) of each channel was stored. This occurred only for signals crossing a threshold which was set individually for each channel. The online data acquisition software was used to store the synchronized data of each system on a PC for further analysis.

The AGET chip, originally designed for the GEM based time projection chambers (TPCs) used in nuclear physics experiments[18], has wide dynamic range and high-precision time and charge measurements. It integrates a charge-sensitive amplifier, a filter shaping circuit, a discriminator, and a switched capacitor array (SCA). The prototype output signal comprised a fast component from the avalanche electron drift and a slow one arising from the motion of the avalanche ions. The latter contributed the most and the signal trailing edge lasted about 100 ns. Therefore the FEE was operated with a 120 fC dynamic range, a 1 μs shaping time and a 100 MHz sampling frequency during the test. Figure 4 shows the output waveform recorded from the incident beam ionization (a) and the Cherenkov photo-electron(b).

The DCMs contained multiple 1 Gbps optical fiber serial link interfaces which allowed to read 1024 channels and was possible to scale up by configuring one DCM as a master while other DCMs in slave mode. Two DCMs were used

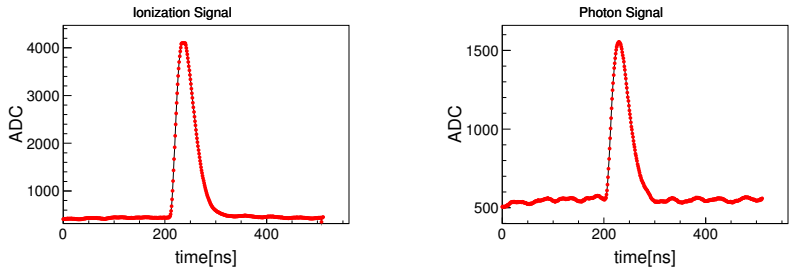

(a) (b)

Figure 4: The recorded waveform from (a) incident electron beam (b) Cherenkov photo-electron.

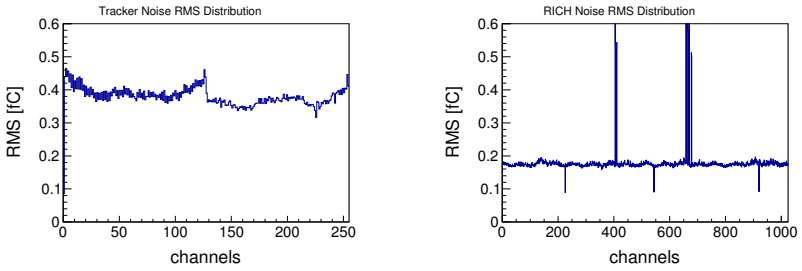

(a) (b)

Figure 5: RMS of noise charge for (a) tracker and (b) RICH.

during the experiments. One was in master mode for RICH prototype with 1024 channels readout and the other one was in slave mode for tracker system with 3×256 channels readout.

Figure 5 shows that the equivalent input noise charge of one tracker and RICH were typically around 0.4 fC and 0.2 fC in RMS (root mean square) for tracker and RICH, respectively.

The HV was provided by three CAEN NDT1471H power supply modules. The HV was monitored throughout data-taking and recorded every 1 minutes. The trip currents were set to $2\,\mu$A. The supplied voltage typically varied by ± 2 V and each channel was calibrated separately. The voltage of tracker MicroMegas were set to 550 V. For RICH prototype, the voltage of the drift mesh, the

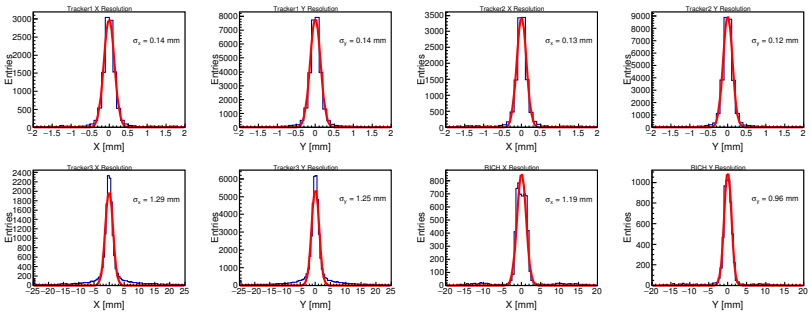

Figure 6: distribution of the residuals between the hit position and extrapolated position.

THGEM up/bottom layer and MicroMegas were 1990 V, 1995 V, 920 V and 570 V, respectively.

4. Reconstruction and Analysis

4.1. Track Reconstruction and Extrapolation

The track reconstruction flow undergoes the following stages: (i) finding where hits are grouped into track candidates for each tracker, (ii) estimate the hit position with the charge centroid method, (iii) track fitting of candidates with linear function, and (iv) extrapolating the optimal track to the RICH prototype.

Figure.6 shows the distribution of the residuals between the hit position and extrapolated position for trackers and RICH(rotated in 30° position). After reconstruction, the spatial resolutions for the first two trackers were about 140 μm, while the resolution of the last tracker was about 1.3 mm mainly because the electron beam was scattered by the RICH detector. For RICH, it is treated as the ionization signal that the cluster must be within 2 pixels ($\approx$ 9 mm) to the extrapolated position and the accumulated charge must be the largest. The resolution σ_y of RICH was improved by a factor of $\sqrt{3}/2$ due to the rotation.

4.2. Cherenkov Angle Reconstruction Algorithm

An analytical Cherenkov reconstruction algorithm was developed. It is an extension from $\beta - Method$[3] from ALICE HMPID with the following hypotheses:

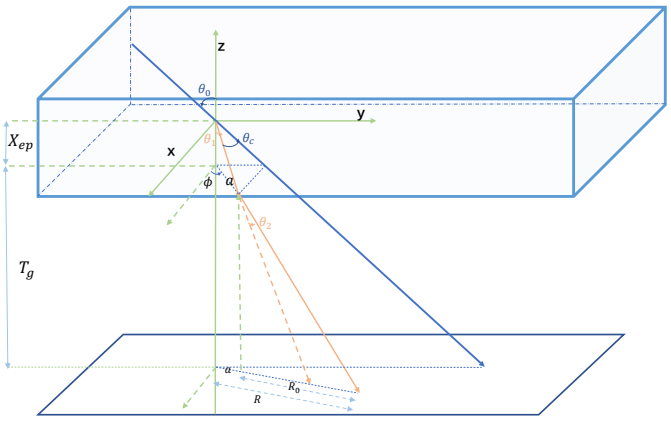

Figure 7: coordinate system, the coordinate system is set up at the center of the radiator. The blue line is the track of the incident electron and the orange line is the Cherenkov photon produced by the electron.

the refractive index for each optical component is taken at the average energy 181 nm(6.85 eV), the photon emission point is nearly at the centre of the track path inside the Chernekov radiator.

Fig.7 illustrates the geometry of the angle reconstruction. Reconstructed Cherenkov angle is obtained by fitting the photon distribution map.

According to cosine theorem and trigonometric functions, we can obtain:

$$a = \frac{-\sqrt{X_{ep}^2 \cos^2\theta_c \sec^4\theta_0 (1 + \cos 2\theta_0 - 2\cos 2\phi \sin^2\theta_0)} + 2X_{ep}\sin\phi\tan\theta_0}{2\cos^2\theta_c \sec^2\theta_0 - 2\sin^2\phi\tan^2\theta_0} \tag{1}$$

where X_{ep} is the starting point of Cherenkov radiation, θ_0 is the angle between electron beam and detector's normal line, θ_c is Cherenkov angle which is equal to $\arccos(1/n\beta)$, n is refractive-index of quartz and β is the velocity of electron in quartz. ϕ is the polar angle in our coordinate system.

Considering refraction process:

$$R = a + |T_g| \tan(\arcsin(\frac{n_1}{n_2}\frac{a}{\sqrt{a^2 + X_{ep}^2}})) \tag{2}$$

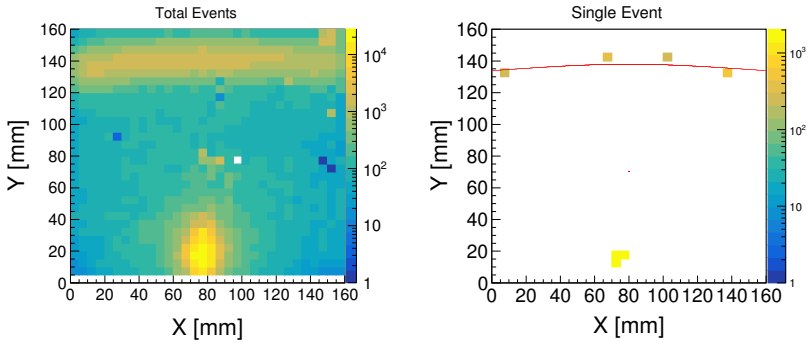

Figure 8: Superimposed events including the beam region and single events.

R denotes the length of the polar axis of the photon after refraction in the plane where the anode plate is located by establishing a polar coordinate system. T_g is the thickness of the gas.

4.3. Analysis results

Typical images of superimposed events and of single events are shown in Fig.8.

The angular resolution of single photon electron (SPE) is affected by the following systematic errors:

(1) The *chromatic error* σ_n, related to the chromatic dispersion of the radiator refractive index n over the detectable energy range of the Cherenkov photon. The photon energy range is about $160 \sim 210\,\mathrm{nm}$ which is determined by the convolution of the CsI photo-cathode quantum efficiency with the transmission of the media traversed by the Cherenkov photons inside the detector, and the refractive index of quartz varies $\approx 7\%$ in this region.

(2) The *geometric error* σ_{geo}, related to the position of the photon emission point uncertainty. This error is proportional to the track path inside the radiator $\frac{L/\cos\theta}{\sqrt{12}}$.

(3) The *localization error* σ_{local}, related to the spatial resolution of the RICH detector. It is determined by the detector characteristics such as pad size. Note that for Cherenkov photon detection, a large fraction of pad clusters

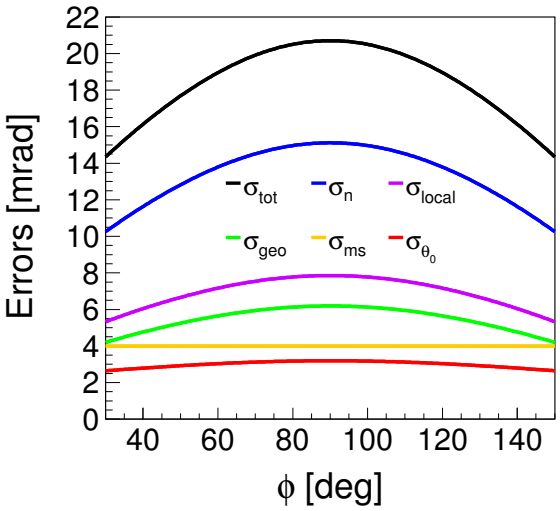

Figure 9: Contributions to the Chernekov angle resolution from each systematic error components for $\theta_0 = 30°$.

is only one pad hit, thus the centroid evaluation is not applicable. This error is estimated by $L_{pad}/\sqrt{12}$.

(4) The *multiple scatteringerror* σ_{ms}, related to the multiple scattering of electron beam in the radiator and its container. This error is estimated by taking the $\sigma_{ms} \sim \delta\theta_{ms}$ where $\delta\theta_{ms} \propto (1/p)\sqrt{L/X_0}$.

(5) The *track incident angle error* σ_{θ_0}, related to the particle incident angle θ_0 and to the precision of the tracking detectors.

Figure 9 shows the distribution of the calculated contributions to the total angular resolution as a function of the azimuthal angle ϕ for the incident angle $\theta_0 = 30°$. The systematic error is dominated by the chromatic error which is intrinsic and contributes about 14 mrad when azimuth angle is 90°. The total calculated error is about 20 mrad.

The analytical reconstruction studies for S.P.E has been carried out with the test-beam data in single particle events. In Fig.10(a) the angular resolution for S.P.E is about 24.07 mrad at $\theta_0 = 30°$. Monte-carlo simulation based on Geant4 [19] has been developed aiming at a better understanding of the experimental

data. Figure 10(b) shows the MC simulated angular resolution for the same configuration. The resolution is about 21.45 mrad and in consistent with the analytical calculation. The different between MC and test beam data is from the non-uniformity of the quantum efficiency, the THGEM and MicroMegas detection efficiency, and so on.

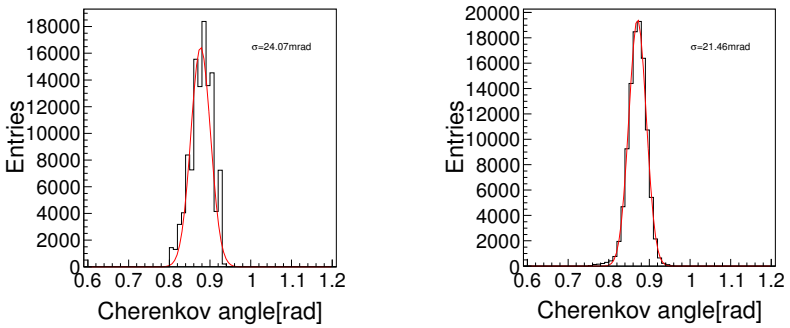

(a) (b)

Figure 10: S.P.E Cherenkov angle resolution of test beam data and MC simulation

The angular resolution has also been tested for tracks with different incident angle with respect to the normal direction. In Fig.11 shows the result for 30° to 45° with 5° step. The angular resolution becomes worse as the incident angle increases. Monte-carlo simulation shows a similar behavior. This can be seen from Eq. 1: when the incident angle θ_0 getting closer to the Chernekov radiation angle θ_c, the spatial resolution will be dominate to determine the value a, thus the angular resolution is getting worse.

5. Conclusion

The STCF is a new generation electron-positron collider. An excellent PID system is vital espeically for the hadrons with momentum up to 2 GeV/c. The hybrid THGEM-MicroMegas detectors with approximately focused radiator design has been adopted as the baseline for the barrel PID detector.

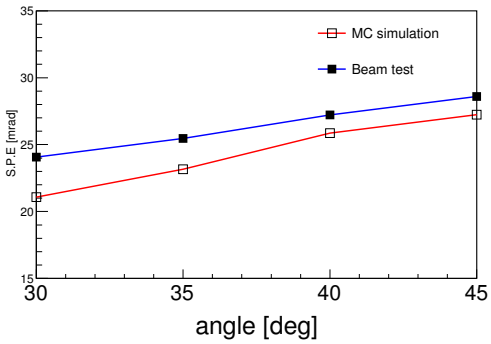

Figure 11: angule resolution as a function of the track incidence

The prototype with the similar design as STCF PID detector has been built and tested with DESY electron beam. The homemade THGEM and Micromegas hybrid detector has been demonstrated to be capable for single photon detection, and presented high gains in the order of 10^5. Additionally the AGET frond-end chips has proven a good performance during the beam test. A new analytical reconstruction algorithm extended from ALICE HMPID $\beta - method$ has been developed. The most relevant parameters for the reconstruction algorithm has been studied using both simulations and beam-test measurements. This algorithm is not valid for large incident angle and a new reconstruction algorithm based on maximum likelihood method is being developed for this purpose.

The optimization of the detector response and the engineering problems related to larger size prototype with liquid C_6F_{14} radiator are presently being investigated.

Acknowledgement

This work was supported by the National Natural Science Foundation of China (Grant Nos. U1732266, 12175241, 12027803), Key Research Program of Frontier Sciences of CAS (Grant No. QYZDB-SSW-SLH039), international partnership program of CAS(Grant No. 211134KYSB20200057). The authors thank Hefei Comprehensive National Science Center for their strong support

and the Double First-Class university project foundation of USTC. The measurements leading to these results have been performed at the Test Beam Facility at DESY Hamburg (Germany), a member of the Helmholtz Association (HGF).

References

References

[1] M. Artuso, R. Ayad, K. Bukin, A. Efimov, C. Boulahouache, E. Dambasuren, S. Kopp, J. Li, G. Majumder, N. Menaa, et al., The cleo rich detector, Nuclear Instruments and Methods in Physics Research Section A: Accelerators, Spectrometers, Detectors and Associated Equipment 554 (1-3) (2005) 147–194.

[2] P. A. Aarnio, P. Abreu, H. Abie, W. Adam, The delphi detector at lep, Nucl. Instrum. Methods Phys. Res., A 303 (CERN-PPE-90-128) (1990) 233–276.

[3] F. Piuz, W. Klempt, L. Leistam, J. De Groot, J. Schükraft, ALICE high-momentum particle identification: Technical Design Report, Technical design report. ALICE, CERN, Geneva, 1998.
URL `https://cds.cern.ch/record/381431`

[4] J. Agarwala, M. Alexeev, C. Azevedo, F. Bradamante, A. Bressan, M. Büchele, M. Chiosso, C. Chatterjee, A. Cicuttin, P. Ciliberti, et al., The mpgd-based photon detectors for the upgrade of compass rich-1 and beyond, Nuclear Instruments and Methods in Physics Research Section A: Accelerators, Spectrometers, Detectors and Associated Equipment 936 (2019) 416–419.

[5] M. Alexeev, R. Birsa, F. Bradamante, A. Bressan, M. Büchele, M. Chiosso, P. Ciliberti, S. Dalla Torre, S. Dasgupta, O. Denisov, et al., Status and progress of the novel photon detectors based on thgem and hybrid mpgd

architectures, Nuclear Instruments and Methods in Physics Research Section A: Accelerators, Spectrometers, Detectors and Associated Equipment 766 (2014) 133–137.

[6] R. Chechik, A. Breskin, C. Shalem, D. Mörmann, Thick gem-like hole multipliers: properties and possible applications, Nuclear Instruments and Methods in Physics Research Section A: Accelerators, Spectrometers, Detectors and Associated Equipment 535 (1-2) (2004) 303–308.

[7] Y. Giomataris, P. Rebourgeard, J. P. Robert, G. Charpak, Micromegas: a high-granularity position-sensitive gaseous detector for high particle-flux environments, Nuclear Instruments and Methods in Physics Research Section A: Accelerators, Spectrometers, Detectors and Associated Equipment 376 (1) (1996) 29–35.

[8] M. Alexeev, R. Birsa, F. Bradamante, A. Bressan, M. Büchele, M. Chiosso, P. Ciliberti, S. Dalla Torre, S. Dasgupta, O. Denisov, et al., Status of the development of large area photon detectors based on thgems and hybrid mpgd architectures for cherenkov imaging applications, Nuclear Instruments and Methods in Physics Research Section A: Accelerators, Spectrometers, Detectors and Associated Equipment 824 (2016) 139–142.

[9] Y.-L. Zhang, H.-R. Qi, B.-T. Hu, H.-Y. Wang, Q. Ou-Yang, Y.-B. Chen, J. Zhang, Z.-W. Wen, A hybrid structure gaseous detector for ion backflow suppression, Chinese Physics C 41 (5) (2017) 056003.

[10] M. Baruzzo, C. Chatterjee, P. Ciliberti, S. Dalla Torre, S. Dasgupta, B. Gobbo, M. Gregori, G. Hamar, S. Levorato, G. Menon, et al., Direct measurements of the properties of thick-gem reflective photocathodes, Nuclear Instruments and Methods in Physics Research Section A: Accelerators, Spectrometers, Detectors and Associated Equipment 972 (2020) 164099.

[11] H.-B. Liu, Y.-H. Zheng, Y.-G. Xie, J.-G. Lu, L. Zhou, B.-X. Yu, A.-W.

Zhang, Z.-H. An, Y.-G. Xie, D. Zhang, et al., Study of the thgem detector with a reflective csi photocathode, Chinese Physics C 35 (4) (2011) 363.

[12] A.-W. Zhang, B.-X. Yu, Y.-G. Xie, H.-B. Liu, Z.-H. An, Z.-G. Wang, X. Cai, X.-L. Sun, F. Shi, J. Fang, et al., Experimental study of a thgem detector with mini-rims, Chinese Physics C 36 (2) (2012) 142.

[13] J. Feng, Z. Zhang, J. Liu, B. Qi, A. Wang, M. Shao, Y. Zhou, A thermal bonding method for manufacturing micromegas detectors, Nuclear Instruments and Methods in Physics Research Section A: Accelerators, Spectrometers, Detectors and Associated Equipment 989 (2021) 164958.

[14] J. Feng, Z. Zhang, J. Liu, M. Shao, Y. Zhou, A novel resistive anode using a germanium film for micromegas detectors, Nuclear Instruments and Methods in Physics Research Section A: Accelerators, Spectrometers, Detectors and Associated Equipment 1031 (2022) 166595.

[15] P. Baesso, D. Cussans, J. Goldstein, The aida-2020 tlu: a flexible trigger logic unit for test beam facilities, Journal of Instrumentation 14 (09) (2019) P09019.

[16] S. Anvar, P. Baron, B. Blank, J. Chavas, E. Delagnes, F. Druillole, P. Hellmuth, L. Nalpas, J. Pedroza, J. Pibernat, et al., Aget, the get front-end asic, for the readout of the time projection chambers used in nuclear physic experiments, in: 2011 IEEE Nuclear Science Symposium Conference Record, IEEE, 2011, pp. 745–749.

[17] C. Li, C. Feng, D. Zhu, S. Liu, Q. An, An optical fiber-based flexible readout system for micro-pattern gas detectors, Journal of Instrumentation 13 (04) (2018) P04013.

[18] E. Pollacco, G. Grinyer, F. Abu-Nimeh, T. Ahn, S. Anvar, A. Arokiaraj, Y. Ayyad, H. Baba, M. Babo, P. Baron, et al., Get: A generic electronics system for tpcs and nuclear physics instrumentation, Nuclear Instruments

and Methods in Physics Research Section A: Accelerators, Spectrometers, Detectors and Associated Equipment 887 (2018) 81–93.

[19] S. Agostinelli, J. Allison, K. a. Amako, J. Apostolakis, H. Araujo, P. Arce, M. Asai, D. Axen, S. Banerjee, G. Barrand, et al., Geant4—a simulation toolkit, Nuclear instruments and methods in physics research section A: Accelerators, Spectrometers, Detectors and Associated Equipment 506 (3) (2003) 250–303.